CD4$^+$ T cells require Ikaros to inhibit their differentiation toward a pathogenic cell fate

Chiara Bernardi[a,b,c,d], Gaëtan Maurer[a,b,c,d], Tao Ye[a,b,c,d,e], Patricia Marchal[a,b,c,d], Bernard Jost[a,b,c,d,e], Manuela Wissler[f], Ulrich Maurer[f,g,h], Philippe Kastner[a,b,c,d,i,1], Susan Chan[a,b,c,d,1], and Céline Charvet[a,b,c,d,1]

[a]Institut de Génétique et de Biologie Moléculaire et Cellulaire, 67404 Illkirch, France; [b]Centre National de la Recherche Scientifique, UMR7104, 67404 Illkirch, France; [c]Institut National de la Santé et de la Recherche Médicale, U1258, 67404 Illkirch, France; [d]Université de Strasbourg, 67000 Strasbourg, France; [e]Plateforme GenomEast, Infrastructure France Génomique, 67404 Illkirch, France; [f]Institute of Molecular Medicine and Cell Research, Albert-Ludwigs-University of Freiburg, 79104 Freiburg, Germany; [g]Spemann Graduate School of Biology and Medicine, Albert-Ludwigs-University of Freiburg, 79104 Freiburg, Germany; [h]BIOSS, Centre for Biological Signalling Studies, 79104 Freiburg, Germany; and [i]Faculté de Médecine, Université de Strasbourg, 67000 Strasbourg, France

Edited by Arthur Weiss, University of California, San Francisco School of Medicine, San Francisco, CA, and approved February 22, 2021 (received for review November 23, 2020)

The production of proinflammatory cytokines, particularly granulocyte-macrophage colony-stimulating factor (GM-CSF), by pathogenic CD4$^+$ T cells is central for mediating tissue injury in inflammatory and autoimmune diseases. However, the factors regulating the T cell pathogenic gene expression program remain unclear. Here, we investigated how the Ikaros transcription factor regulates the global gene expression and chromatin accessibility changes in murine T cells during Th17 polarization and after activation via the T cell receptor (TCR) and CD28. We found that, in both conditions, Ikaros represses the expression of genes from the pathogenic signature, particularly *Csf2*, which encodes GM-CSF. We show that, in TCR/CD28-activated T cells, Ikaros binds a critical enhancer downstream of *Csf2* and is required to regulate chromatin accessibility at multiple regions across this locus. Genome-wide Ikaros binding is associated with more compact chromatin, notably at multiple sites containing NFκB or STAT5 target motifs, and STAT5 or NFκB inhibition prevents GM-CSF production in Ikaros-deficient cells. Importantly, Ikaros also limits GM-CSF production in TCR/CD28-activated human T cells. Our data therefore highlight a critical conserved transcriptional mechanism that antagonizes GM-CSF expression in T cells.

Ikaros | GM-CSF | IL-17 | proinflammatory cytokines | pathogenicity

Upon antigen recognition and depending on the cytokine context, naive CD4$^+$ T cells polarize into different effector populations. CD4$^+$ T cells become IL-17–secreting Th17 cells in the presence of IL-6 and TGFβ1, and the induction of the RORγt transcription factor is central to this process (1, 2). IL-17$^+$ T cells are important for clearing fungi and extracellular bacterial infections and have been implicated in gut homeostasis. They are often called conventional (c), or "nonpathogenic," Th17 cells because they do not induce tissue inflammation (3) and possess immunoregulatory functions through IL-10 secretion (4). On the other hand, CD4$^+$ T cells become "pathogenic" (p) Th17 cells with the addition of IL-23, or in the presence of IL-23, IL-1β and IL-6 (5, 6). pTh17 cells promote autoimmunity and have been reported to induce experimental autoimmune encephalomyelitis (EAE), the murine model for multiple sclerosis, via their production of proinflammatory cytokines (5–8). CD4$^+$ T cells can also differentiate into pathogenic Th1 and Th-GM cells which themselves contribute to autoimmune disease progression (9–11). Thus, naive CD4$^+$ T cells can polarize into multiple types of pathogenic effector cells with unique phenotypes. All of them are characterized by the high production of the proinflammatory cytokine, granulocyte-macrophage colony-stimulating factor (GM-CSF).

Indeed, GM-CSF production is tightly associated with T cell pathogenicity. Local GM-CSF production by T cells is closely linked to tissue inflammation in neuropathological disorders like multiple sclerosis (12, 13). High GM-CSF production has also been observed in patients with Coronavirus disease 2019 (Covid-19) (14–16), suggesting a potential target for treatment. How GM-CSF expression is regulated is only partially understood, but this knowledge is of considerable importance.

GM-CSF is encoded by the *Csf2* gene, which requires the T cell receptor (TCR) and CD28 pathways to be expressed in T cells (17) as well as IL-23 and IL-7 signaling in some cases (6–8, 10). Transcription of the *Csf2* gene is controlled by the *Csf2* promoter and two enhancers, with one located ~1.5 kb upstream and a conserved noncoding sequence (CNSa) ~34 kb downstream of the transcriptional start site (18–20). The promoter contains binding sequences for the transcription factors NFAT, NFκB, AP-1, and Brg1 and is sensitive to changes in chromatin accessibility (21–28). *Csf2* promoter activity is potentiated upon NFAT and AP-1 binding to the upstream enhancer and NFκB and Brg1 binding to the CNSa region (19, 20). In addition, STAT5 and the Foxo3-Eomes axis have been described to be important for GM-CSF production in Th-GM and Th1 cells, respectively, and for influencing the pathogenic potential of these cells (9, 10, 29). Most of the factors identified so far have been transcriptional activators. However, given the centrality of this cytokine in inflammation and autoimmunity, we hypothesized that negative regulators of *Csf2*

Significance

The production of proinflammatory cytokines, particularly granulocyte-macrophage colony-stimulating factor, by CD4$^+$ T cells is a key process for amplifying immune responses but can also lead to harmful tissue damage in pathologies like multiple sclerosis and Covid-19. Correctly controlling the expression of proinflammatory cytokines is therefore of major interest. However, the pathogenic signature of CD4$^+$ T cells relies on a transcriptional program that is thus far poorly understood. Here, we identified the transcription factor Ikaros as an essential transcriptional repressor of proinflammatory cytokine gene expression. Our work identifies a critical molecular pathway regulating the pathogenic program of CD4$^+$ T cells and brings new perspectives for potential therapies of autoimmune and inflammatory diseases.

Author contributions: C.B., G.M., P.K., S.C., and C.C. designed research; C.B., G.M., P.M., B.J., M.W., U.M., P.K., and C.C. performed research; C.B., G.M., T.Y., P.K., S.C., and C.C. analyzed data; and C.B., G.M., P.K., S.C., and C.C. wrote the paper.

The authors declare no competing interest.

This article is a PNAS Direct Submission.

[1]To whom correspondence may be addressed. Email: scpk@igbmc.fr or charvetc@igbmc.fr.

This article contains supporting information online at https://www.pnas.org/lookup/suppl/doi:10.1073/pnas.2023172118/-/DCSupplemental.

Published April 23, 2021.

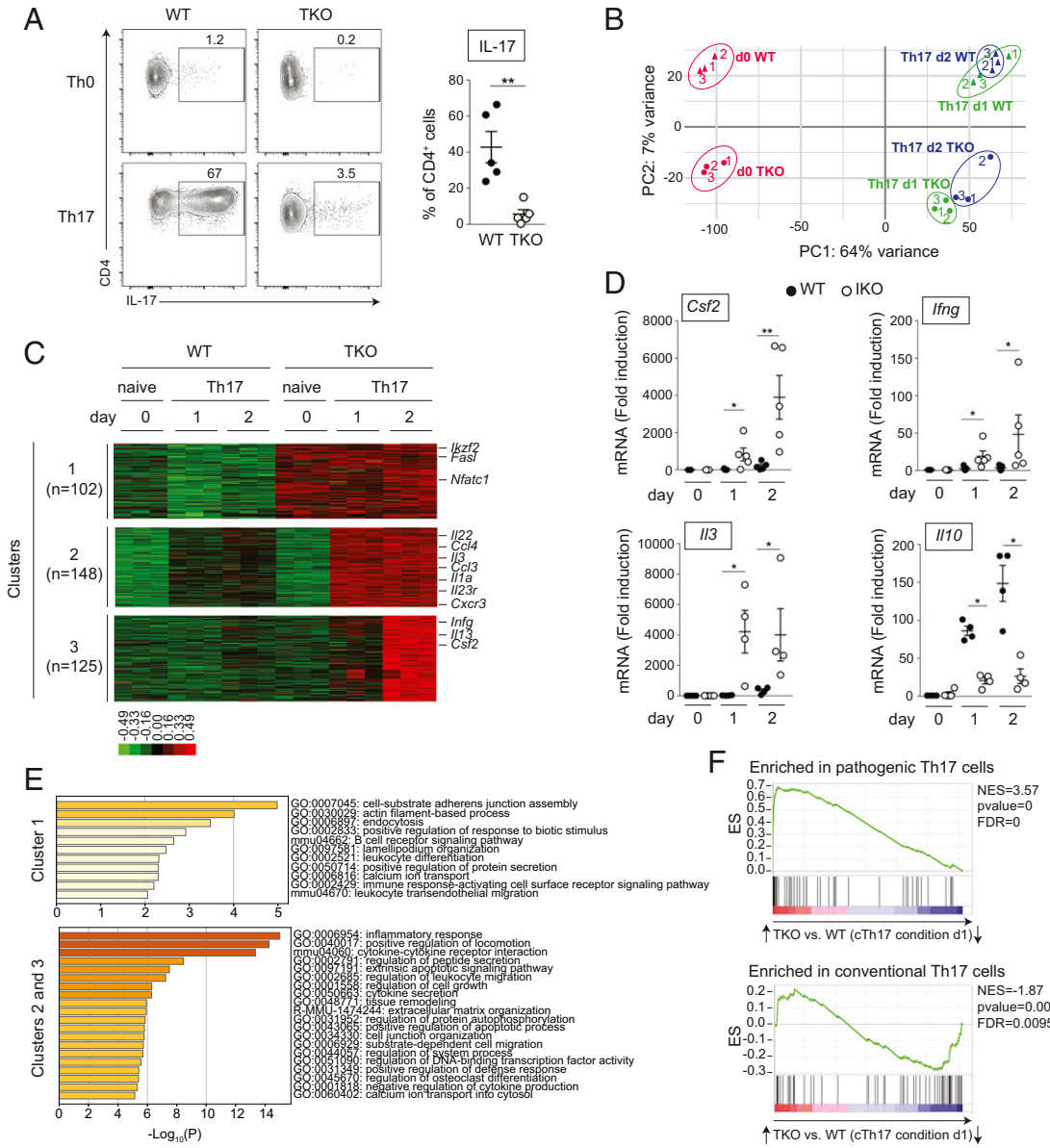

Fig. 1. Loss of Ikaros induces a pathogenic gene expression program. (*A*, *Left*) Representative contour plots of IL-17 and CD4 expression in WT and TKO CD4$^+$ cells stimulated for 3 d in Th17 or Th0 conditions. (*A*, *Right*) Proportion of WT or TKO IL-17$^+$ cells among CD4$^+$ cells from 3 d in Th17 cultures (n = 5; mean ± SEM). (*B*) PCA using expression data (microarray) from WT and TKO CD4$^+$ cells at day 0 and day 1 to 2 in Th17 cultures. The graph shows the first two principal components. (*C*) Heatmaps of three clusters of genes that were specifically increased in TKO cells compared to WT (K-means clustering). (*D*) RT-qPCR analysis of *Csf2*, *Ifng*, *Il3*, and *Il10* mRNA expression in either naive CD4$^+$ T cells (day 0) or naive CD4$^+$ T cells cultured in Th17 polarizing condition with QVD-OPh for 1 or 2 d (n = 4 to 5; mean ± SEM). (*E*) Metascape analysis of Gene Ontology term enrichment of genes in cluster 1 to 3 described in *C*. (*F*) Gene set enrichment analysis enrichment plots of genes enriched in pathogenic Th17 cells (pTh17; *Top*) or conventional Th17 cells (cTh17; *Bottom*) among genes up- or down-regulated by Ikaros at day 1. Gene sets correspond to 106 genes enriched in pTh17 cells and 143 genes enriched in cTh17 cells (6). ES, enrichment score; NES, normalized enrichment score; FDR, false discovery rate. Statistical significance was analyzed by a Mann–Whitney U test (*$P \leq 0.05$ and **$P \leq 0.01$).

expression must be equally important for the regulation of this gene.

Here, we characterize the role of the Ikaros transcription factor in regulating GM-CSF production during T cell activation and Th17 polarization. We show that Ikaros is a repressor of *Csf2* messenger RNA (mRNA) expression and that Ikaros is required to limit the pathogenic gene expression program in activated T cells.

Results

Ikaros Represses a Pathogenic Gene Expression Program in CD4$^+$ T Cells. Up to now, the role of Ikaros in Th17 cell differentiation and IL-17 production has been unclear. IL-17 expression by cTh17-polarized cells is severely blunted in germline Ikaros null mice (30) but seems inconsistently affected in animals where Ikaros is deleted in peripheral T cells (31). In contrast, IL-17 production is enhanced in Th17 cells from mice with a targeted deletion of the fourth DNA-binding zinc finger (ZnF4) of Ikaros (32). To clarify the role of Ikaros in Th17 polarization, we studied Ik$^{f/f}$ CD4-Cre$^+$ (TKO) mice where *Ikzf1* is selectively deleted in T cells (*SI Appendix*, Fig. S1*A*) (33). Purified naive CD4$^+$CD25$^-$CD44$^{lo/-}$TCRγδ$^-$NK1.1$^-$ T (TN) cells from TKO and wild-type (WT) (Ik$^{f/f}$ CD4-Cre$^-$) lymph nodes were stimulated with anti-CD3 and anti-CD28 antibodies (Ab) alone ("Th0 conditions") or in the presence of IL-6 and TGFβ1 ("Th17 conditions"). Cytoplasmic IL-17 production was

analyzed after 3 d by flow cytometry (Fig. 1*A*). In these cultures, the majority of WT cells were induced to make IL-17 under Th17 compared with Th0 conditions (67% versus 1.2%, respectively), as expected, while TKO cells made little to no IL-17 in either condition. Therefore, naive $CD4^+$ T cells cannot produce IL-17 in response to Th17 cell polarization without Ikaros.

To understand the Th17 response in the absence of Ikaros, we evaluated the gene expression profiles of WT and TKO naive $CD4^+$ T cells cultured in Th17 conditions (and in the presence of anti-IFNγ and anti–IL-4 neutralizing Abs to block indirect effects) over time (days 0, 1, and 2) by microarray analysis. These experiments revealed that WT and TKO cells responded similarly in general to Th17 conditions, as the majority of the up- (>3,000) and down-regulated (>1,500) genes overlapped between genotypes at days 1 and 2 [fold change (FC) > 1.42] (*SI Appendix*, Fig. S1 *B* and *C*). Still, there were clear differences. Principal component analysis (PCA) revealed that WT and TKO cells were distinct at every timepoint (Fig. 1*B*). Among the up-regulated genes, Th17-associated genes were less up-regulated in TKO cells with time, such as *Il17a*, *Il17f*, *Il21*, and *Rorc* (clusters 11 and 12) (*SI Appendix*, Fig. S1*B*). *Il17a* and *Rorc* mRNA levels were confirmed by qRT-PCR (*SI Appendix*, Fig. S1*D*). Cell cycle–related genes were also less induced in TKO cells (cluster 18) (*SI Appendix*, Fig. S1 *B* and *E*).

Interestingly, three clusters of genes were ectopically expressed in Th17 conditions in the absence of Ikaros (Fig. 1*C*). Cluster 1 contained genes that were constitutively expressed in naive TKO $CD4^+$ T cells and remained expressed over time; it included genes encoding Helios (*Ikzf2*) and NFATc1 (*Nfatc1*). Clusters 2 and 3 contained genes that were similarly expressed in WT and TKO cells at day 0 but were strongly induced in the mutant cells at day 1 or 2; they included genes encoding proinflammatory cytokines (e.g., *Ifng*, *Csf2*, *Il1a*, *Il3*, *Il13*, *Il22*, *Ccl3*, and *Ccl4*) or their receptors (e.g., *Il23r* and *Cxcr3*) (Fig. 1 *C*–*E*). On the other hand, the anti-inflammatory cytokine gene *Il10* was induced but less up-regulated in TKO cells (cluster 12) (*SI Appendix*, Fig. S1*B* and Fig. 1*D*).

Since proinflammatory cytokines are characteristic of pathogenic Th17 cells, we performed a gene set enrichment analysis with the most differentially expressed genes between TKO and WT samples and compared them with genes highly expressed in pTh17 or cTh17 cells (6). This showed a strong and direct correlation between TKO T cells and pTh17, but not cTh17, cells (Fig. 1*F* and *SI Appendix*, Fig. S2*A*), suggesting that TKO $CD4^+$ T cells resemble pTh17 cells after stimulation. We also compared TKO cells with the recently described Th-GM cells (10) and Th17 cells from the central nervous system of mice with EAE (34) and found a strong correlation between the genes differentially expressed in TKO and those expressed in these T cell populations (*SI Appendix*, Fig. S2 *B* and *C*).

Collectively, these results indicated that activated $CD4^+$ T cells cannot produce IL-17 and enter a proinflammatory gene program in the absence of Ikaros.

Ikaros Is Required in $CD4^+$ T Cells to Coordinate Cytokine Responses. To determine if Ikaros loss in the periphery impacts the state of naive $CD4^+$ T cells to lead to the abnormal response, we acutely deleted the *Ikzf1* alleles in $Ik^{f/f}$ R26-CreERT2$^+$ (IKO) and $Ik^{f/f}$ R26-CreERT2$^-$ (WT) mice, which were injected with tamoxifen for 3 d followed by 3 d of rest (*SI Appendix*, Fig. S3*A*). This protocol did not alter the naive $CD4^+$ T cell compartment in numbers or phenotype (*SI Appendix*, Fig. S3*B*). Naive $CD4^+$ T cells were stimulated with anti-CD3 and anti-CD28 Abs in the absence or presence of IL-6 and increasing concentrations of TGFβ1, and IL-17 production was measured 3 d later (Fig. 2*A*). WT IL-17$^+$ cells were easily detected in wells with low concentrations of TGFβ1 (0.0017 to 0.03 ng/mL), and their numbers decreased as TGFβ1 concentrations went up, as expected (35). In contrast, IKO IL-17$^+$ cells were barely detected in all conditions, similar to TKO cells. Thus, naive peripheral $CD4^+$ T cells need Ikaros to become Th17 cells.

High TGFβ1 concentrations induce the differentiation of Foxp3$^+$ regulatory T (Treg) cells (36), and naive $CD4^+$ T cells may preferentially differentiate into Treg cells in the absence of Ikaros. We therefore measured the appearance of Foxp3$^+$ T cells in Th17 conditions as described above. This showed that Foxp3$^+$ cells were produced in the WT samples at the higher TGFβ1 concentrations (0.5 to 8 ng/mL), but they were not observed in the IKO wells (*SI Appendix*, Fig. S3*C*). Thus, Ikaros is required for the appearance of both Th17 and Treg cells following IL-6 and TGFβ1 stimulation.

As the mRNA of proinflammatory cytokines were up-regulated in the Ikaros knockout T cells, we assessed GM-CSF production in naive IKO $CD4^+$ T cells stimulated in Th0 or Th17 conditions. Strikingly, more IKO cells made GM-CSF, and more GM-CSF was made per cell, regardless of stimulation, and at all concentrations of TGFβ1 tested compared with WT (Fig. 2 *B* and *C*). IKO $CD4^+$ T cells also produced more IFNγ (*SI Appendix*, Fig. S3*D*), confirming a general deregulation of proinflammatory cytokine production in the absence of Ikaros. To determine if these results were due to Ikaros, or the indirect effects of IFNγ and IL-4 produced in these cultures (37), we performed the experiments in the presence of neutralizing Abs against these cytokines. This treatment inhibited endogenous IFNγ production (*SI Appendix*, Fig. S3*E*), but there was no detectable effect on the generation of IKO IL-17$^+$, Foxp3$^+$, or GM-CSF$^+$ cells (*SI Appendix*, Fig. S3 *F*–*H*). Thus, Ikaros promotes IL-17 and inhibits proinflammatory cytokine production during Th17 polarization.

In the course of these experiments, we noticed more cell death in the Ikaros null cultures, a process that was reduced by the addition of the pan-caspase inhibitor QVD-OPh (*SI Appendix*, Fig. S4*A*), suggesting death by apoptosis. Since *Fasl* mRNA was up-regulated in stimulated TKO T cells (Fig. 1*C*), we asked if FasL signaling promoted IKO cell death, and perhaps the overproduction of GM-CSF$^+$ cells, since this pathway is associated with the production of proinflammatory cytokines (38). To address these questions, we first measured *Fasl* mRNA in naive WT and IKO $CD4^+$ T cells after 0 to 2 d of culture in Th0 or Th17 conditions; *Fasl* mRNA was easily detected in the IKO cells within 1 d of stimulation in either condition compared with WT (*SI Appendix*, Fig. S4*B*). Surface FasL was also increased on IKO cells (*SI Appendix*, Fig. S4*C*). We then cultured naive WT and IKO $CD4^+$ T cells in Th0 conditions in the absence or presence of anti-FasL neutralizing Abs and analyzed the cells for annexin V and propidium iodide positivity after 2 d. IKO cells had significantly less annexin V$^+$ cells when FasL signaling was blocked (*SI Appendix*, Fig. S4*D*). To determine if FasL deregulation promotes GM-CSF expression in Ikaros null cells, we cultured naive WT and IKO T cells in Th0 conditions, in the presence of anti-FasL Abs, and measured GM-CSF expression. Interestingly, while the anti-FasL Ab blocked the appearance of WT GM-CSF$^+$ cells, as expected, it had little effect on IKO cells (*SI Appendix*, Fig. S4*E*). Indeed, the number of IKO GM-CSF$^+$ cells seemed to increase when FasL signaling was blocked. Thus, Ikaros promotes cell survival by preventing *Fasl* up-regulation but blocks proinflammatory cytokine production via a different mechanism. In addition, QVD-OPh was included in the experiments below, unless specified, to maintain cell viability.

To determine if Ikaros is directly required during T cell polarization, we deleted *Ikzf1* in vitro, during the culture period, in $CD4^+$ T cells of untreated WT and IKO mice. Cells were cultured in Th0 or Th17 conditions and simultaneously treated with 4-hydroxytamoxifen (4-OHT) or ethanol (EtOH). Ikaros, GM-CSF, and IL-17 expression were analyzed after 1 to 3 d of culture (*SI Appendix*, Fig. S5). In these cultures, loss of Ikaros was observed in the large majority of cells after 2 d of 4-OHT treatment.

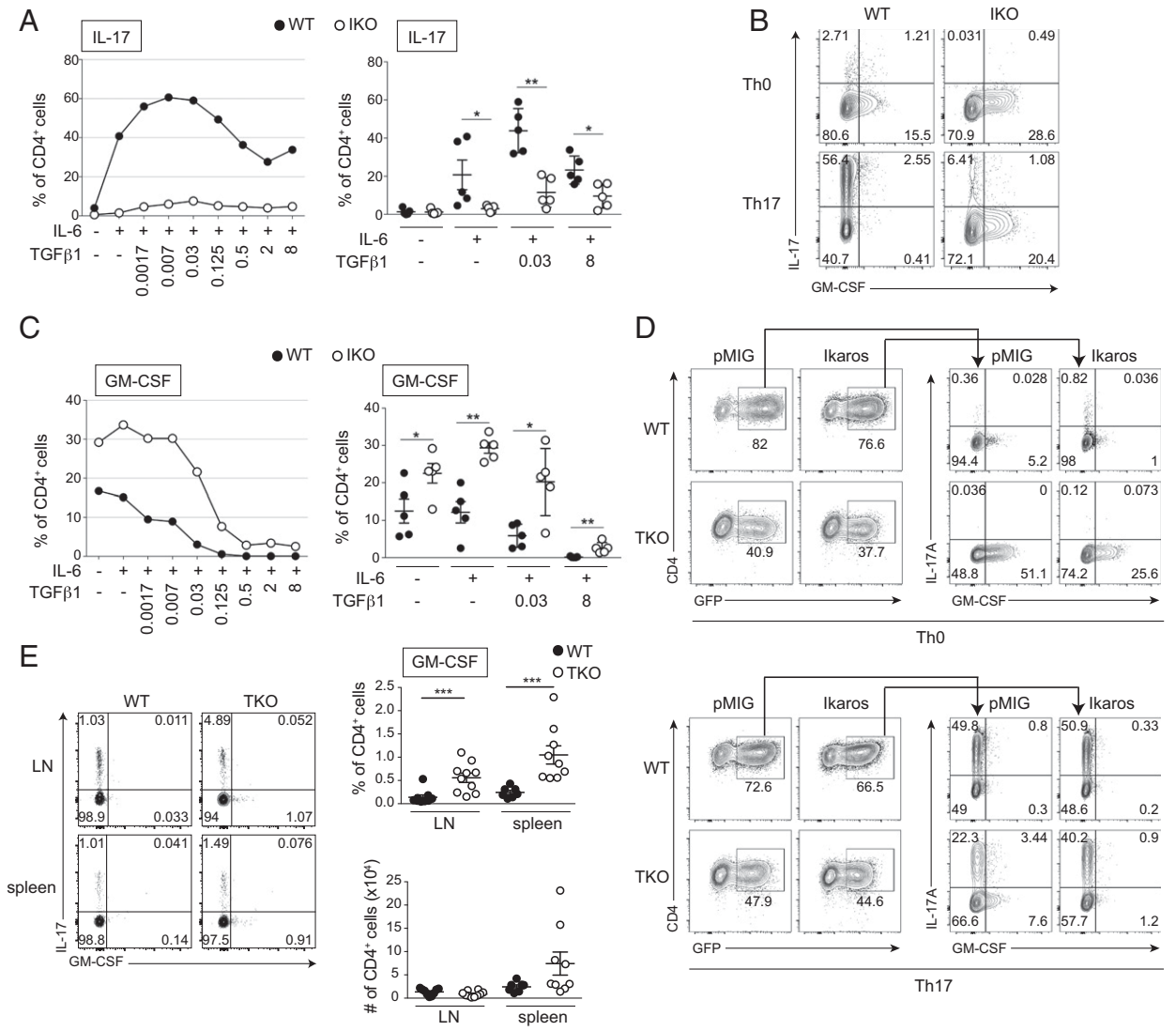

Fig. 2. Ikaros limits the expression of GM-CSF in Th17 polarizing conditions. (*A*, *Left*) Representative graph of the proportions of IL-17$^+$ cells in activated WT and IKO naive LN CD4$^+$ T cells cultured with anti-CD3 and anti-CD28 Abs and different amounts of TGFβ1 and constant IL-6 for 3 d, as indicated. (*A*, *Right*) Graph showing the proportions of WT and IKO IL-17$^+$ cells among CD4$^+$ T cells in 3 d cultures, as indicated ($n = 5$; mean ± SEM). (*B*) Representative contour plot showing IL-17 and GM-CSF expression in WT and IKO CD4$^+$ cells after 3 d of culture in Th0 or Th17 conditions. (*C*, *Left*) Representative graph showing the percentage of GM-CSF$^+$ cells in WT and IKO LN CD4$^+$ cells cultured as in *A*. (*C*, *Right*) Graph showing the proportions of GM-CSF$^+$ CD4$^+$ T cells ($n = 5$; mean ± SEM). (*D*) Naive LN CD4$^+$ T cells from WT and TKO mice, cultured in Th0 or Th17 conditions for 24 h and subjected to two rounds of infection with pMIG or Ikaros/pMIG in the presence of QVD-OPh. A representative panel of GFP expression at day 3, and an expression of IL-17 and GM-CSF in live GFP$^+$ cells in Th0 (*Top*) or Th17 (*Bottom*) condition ($n = 2$) are shown. (*E*, *Left*) Representative contour plot of ex vivo GM-CSF–expressing cells in WT and TKO CD4$^+$ T cells in LN and spleen. (*E*, *Right*) Percentage of GM-CSF$^+$ cells among CD4$^+$ T cells from LN ($n = 10$) or spleen ($n = 9$) from WT and TKO mice and cell counts of GM-CSF$^+$ cells among WT and TKO CD4$^+$ T cells from LN ($n = 10$) or spleen ($n = 9$) of WT and TKO mice (mean ± SEM). Statistical significance was analyzed by a Mann–Whitney *U* test (*$P \leq 0.05$, **$P \leq 0.01$, ***$P \leq 0.001$).

GM-CSF was easily detected in the Ikaros$^{lo/-}$ IKO cells after 3 d of Th0 or Th17 stimulation compared with Ikaros sufficient cells (*SI Appendix*, Fig. S5*A*), though it was less robust in the Th17 cultures due probably to the inhibition of GM-CSF production by exogenous TGFβ1 (8). In contrast, IL-17 production decreased with Ikaros loss in the IKO cells, starting at day 2 in Th17 conditions (*SI Appendix*, Fig. S5*B*). These results indicated that Ikaros loss immediately results in the disappearance of cTh17 and the appearance of pTh17 cells. In a complementary experiment, we retrovirally expressed Ikaros [and green fluorescent protein (GFP)] or GFP only (pMIG) in naive WT and TKO CD4$^+$ T cells during Th0- or Th17-inducing conditions (Fig. 2*D*). In WT cells cultured in Th17 conditions, ectopic Ikaros slightly enhanced IL-17 production but had no effect on GM-CSF expression. In TKO cells, however, Ikaros re-expression rescued IL-17 production in Th17 conditions and reduced GM-CSF in both Th0 and Th17 conditions. These results demonstrated that Ikaros promotes cTh17 polarization even in cells where Ikaros was deleted in the thymus.

To determine if T cell homeostasis in vivo is affected by Ikaros, we analyzed the T cell populations in TKO mice. Mutant mice showed decreases in total lymph node (LN) cellularity and CD4$^+$ and CD8$^+$ T cell numbers compared with WT (*SI Appendix*, Fig. S6 *A* and *B*), though splenic T cells seemed unaffected. The frequencies of CD4$^+$ T cells were also lower. In contrast, B cell numbers were unchanged, but their frequencies were higher in the TKO LNs (*SI Appendix*, Fig. S6*C*). In addition, naive TKO CD4$^+$ T cells were significantly decreased in numbers and frequencies compared with WT (*SI Appendix*, Fig. S6 *D* and *E*), while TKO

effector CD4$^+$ T cells were increased in frequencies (*SI Appendix*, Fig. S6*F*). Interestingly, IL-7Rα levels were reduced on naive TKO CD4$^+$ T cells (*SI Appendix*, Fig. S4*G*), suggesting a possible defect in cell survival. To determine if Ikaros null T cells produced more proinflammatory cytokines in vivo, we evaluated the production of IL-17 and GM-CSF in freshly isolated WT and TKO cells. These experiments indicated that more LN and splenic TKO CD4$^+$T cells, and not CD8$^+$, were consistently and selectively positive for GM-CSF (Fig. 2*E* and *SI Appendix*, Fig. S7*A*). On the other hand, IL-17 production was increased only in frequency in TKO LN CD4$^+$ T cells (*SI Appendix*, Fig. S7*B*). These results suggested that Ikaros deficiency is closely associated with an increase in GM-CSF production in vivo.

Altogether, our results showed that naive CD4$^+$ T cells can become IL-17– or GM-CSF–producing cells depending on the stimulation and their intrinsic levels of Ikaros—IL-17 expression requires high Ikaros levels, while GM-CSF is induced in cells that have lost Ikaros.

Ikaros Is Essential to Limit the Pathogenic Phenotype of CD4$^+$ T Cells and Promotes Their Proliferation upon Activation. Because GM-CSF is induced in Ikaros null cells cultured in Th0 conditions, we explored its activation requirements. Naive WT and IKO CD4$^+$ T cells were isolated from tamoxifen-treated mice and cultured in the absence of TCR stimulation (but maintained in IL-7 to help survival) with anti-CD3 Abs alone or with anti-CD3 + anti-CD28 Abs. GM-CSF and IL-17 levels were measured over 3 d (Fig. 3*A* and *SI Appendix*, Fig. S8*A*). In the absence of TCR stimulation, WT and IKO cells did not make GM-CSF nor IL-17. Indeed, cells from either genotype did not make IL-17 in any of these conditions. However, some WT cells were GM-CSF$^+$ after 3 d of anti-CD3 + anti-CD28 stimulation. Strikingly, a large number of IKO cells made GM-CSF in response to either anti-CD3 or anti-CD3 + anti-CD28 at day 3. These results indicated that Ikaros null T cells needed only TCR stimulation to make GM-CSF, while WT cells required costimulatory CD28 signals, suggesting that Ikaros is required to set the activation threshold for proinflammatory cytokine production in CD4$^+$ T cells.

To determine why Ikaros null T cells respond so differently to TCR and CD28 stimulation, we analyzed the transcriptomes of naive WT and TKO CD4$^+$ T cells activated for 0 to 2 d in Th0 conditions by RNA sequencing (RNA-seq). Three samples were analyzed per condition. PCA of the expressed genes indicated that, globally, freshly isolated WT and TKO cells resembled each other, while activated cells of both genotypes clustered together (PC1; Fig. 3*B*), indicating that cell activation causes the biggest differences in gene expression. Among the up-regulated genes upon T cell activation (*SI Appendix*, Fig. S8*B*), some clusters (i.e., clusters 14, 18, and 19) were less induced in the mutant cells. Similar results were observed among the down-regulated genes (*SI Appendix*, Fig. S8*C*), where genes from a few clusters were less down-regulated (i.e., clusters 7 and 9–11) in TKO cells. WT cells were also distinct from TKO cells (PC2; Fig. 3*B*). Differentially expressed genes that were up-regulated only in the TKO cells included those that were also up-regulated in Th17 conditions, such as genes encoding proinflammatory cytokines or their receptors (e.g., *Csf2*, *Csf1*, *Ifng*, *Il23a*, *Il3*, *Il1a*, *Il15ra*, and *Il2rb*); *Nlrp3*, associated with the inflammasome pathway; and *Foxo3* (Fig. 3 *C* and *D*). *Tbx21*, encoding T-bet, an activator of Th1 polarization, was also up-regulated, and Eomes, another member of the T-box superfamily, was less down-regulated (Cluster 7, *SI Appendix*, Fig. S8*C*), suggesting that the transcriptomic signature of the mutant cells resemble the one of pTh1 cells. In direct correlation, Metascape analysis revealed the top pathways to be associated with cytokine signaling, actin cytoskeleton organization, and migration (Fig. 3*E* and *SI Appendix*, Fig. S9).

We also observed that cell cycle–related genes responded slower to activation and were less up-regulated in Ikaros null cells compared with WT (cluster 18; *SI Appendix*, Fig. S8*B*). This suggested that the proliferative response is impaired in the absence of Ikaros. To investigate this issue, we stimulated naive CD4$^+$ T cells from tamoxifen-treated WT and IKO mice in Th0 and Th17 conditions and measured their division rates and kinetics of cytokine production. We found that IKO cells divided less than WT cells in both conditions, a phenotype that was most striking in Th0 conditions, where the majority of Ikaros null cells divided two cycles less than WT cells (*SI Appendix*, Fig. S10*A*). To correlate cytokine production with cell cycle, we evaluated the percentage of GM-CSF$^+$ and IL-17$^+$ cells at every division after a 3 d culture. This showed that GM-CSF was detected in low proliferating, while IL-17 was observed in high proliferating, IKO cells (*SI Appendix*, Fig. S10 *B* and *C*), revealing, thus, that IL-17 and GM-CSF are produced by different cell populations.

Together, these results indicate that Ikaros represses the appearance of a specific and distinct proinflammatory cytokine-producing CD4$^+$ T cell population in response to activation.

Loss of Ikaros Alters the T Cell Epigenome. To determine how Ikaros influences chromatin accessibility, we studied the epigenome of WT and TKO CD4$^+$ T cells after Th0 activation over a 2 d period by assay for transposase-accessible chromatin sequencing (ATAC-seq). Three samples were analyzed for each condition. A total of 158,327 ATAC-seq peaks was identified for all conditions combined. The chromatin accessibility signatures of the different populations were analyzed by PCA (Fig. 4*A*), which separated the samples along lines similar to their RNA-seq profiles (Fig. 3*B*). Most of the ATAC-seq peaks were similar between WT and TKO chromatin (Fig. 4*B*), suggesting that they were Ikaros independent. A small percentage showed increased or decreased accessibility in the TKO samples compared with WT, but the ratios of up versus down were similar between different days of culture (*SI Appendix*, Fig. S11*A* and Fig. 4*C*). The genes with increased ATAC-seq peaks over time included many encoding proinflammatory cytokines and *Fasl* (*SI Appendix*, Fig. S11*B*). Most of the peaks were found in gene introns or intergenic regions, and this was not changed with the loss of Ikaros (*SI Appendix*, Fig. S11*C*). The majority of the regions with increased accessibility was correlated with genes whose expression levels were increased in the TKO cells (*SI Appendix*, Fig. S11*D* and Fig. 4*D*) and included, among others, proinflammatory genes. Interestingly, the up and down changes in ATAC-seq peak signals were frequently observed within the same locus as was observed for the *Csf2*, *Fasl*, *Il3*, and *Ifng* genes (Fig. 4*E* and *SI Appendix*, Fig. S11*E*), highlighting the complexity of gene regulation. Some of these changes were seen at day 0 in freshly isolated cells, while others were induced upon Th0 activation. These results indicated that increased chromatin accessibility correlates with increased gene expression in Ikaros null cells.

To determine if specific biological pathways are affected by Ikaros loss, we evaluated the ATAC-seq peaks that were greatly increased or decreased (Log_2FC TKO/WT > +2 or < −2; p-value adjusted [padj] ≤ 0.01) in these samples. Gene ontology analysis revealed that few pathways were significantly altered at day 0 and after 1 d of activation (*SI Appendix*, Fig. S12*A*). However, the genes associated with the STAT5 and NFκB pathways displayed some of the highest increases in ATAC-seq peak signals after 2 d of activation (Fig. 4*F*). We then searched for Ikaros-, STAT5-, and NFκB-binding motifs under the peaks that were either increased (TKO) or decreased (WT) in TKO chromatin compared with WT. This showed that, under the peaks that were increased in TKO chromatin, the Ikaros and STAT5 motifs were selectively overrepresented at all timepoints, while RelA (p65) motifs were overrepresented only upon TCR + CD28 stimulation (*SI Appendix*, Fig. S12*B* and Fig. 4*G*). Together, these analyses suggest a molecular significance for Ikaros, STAT5, and RelA motifs in TKO cells.

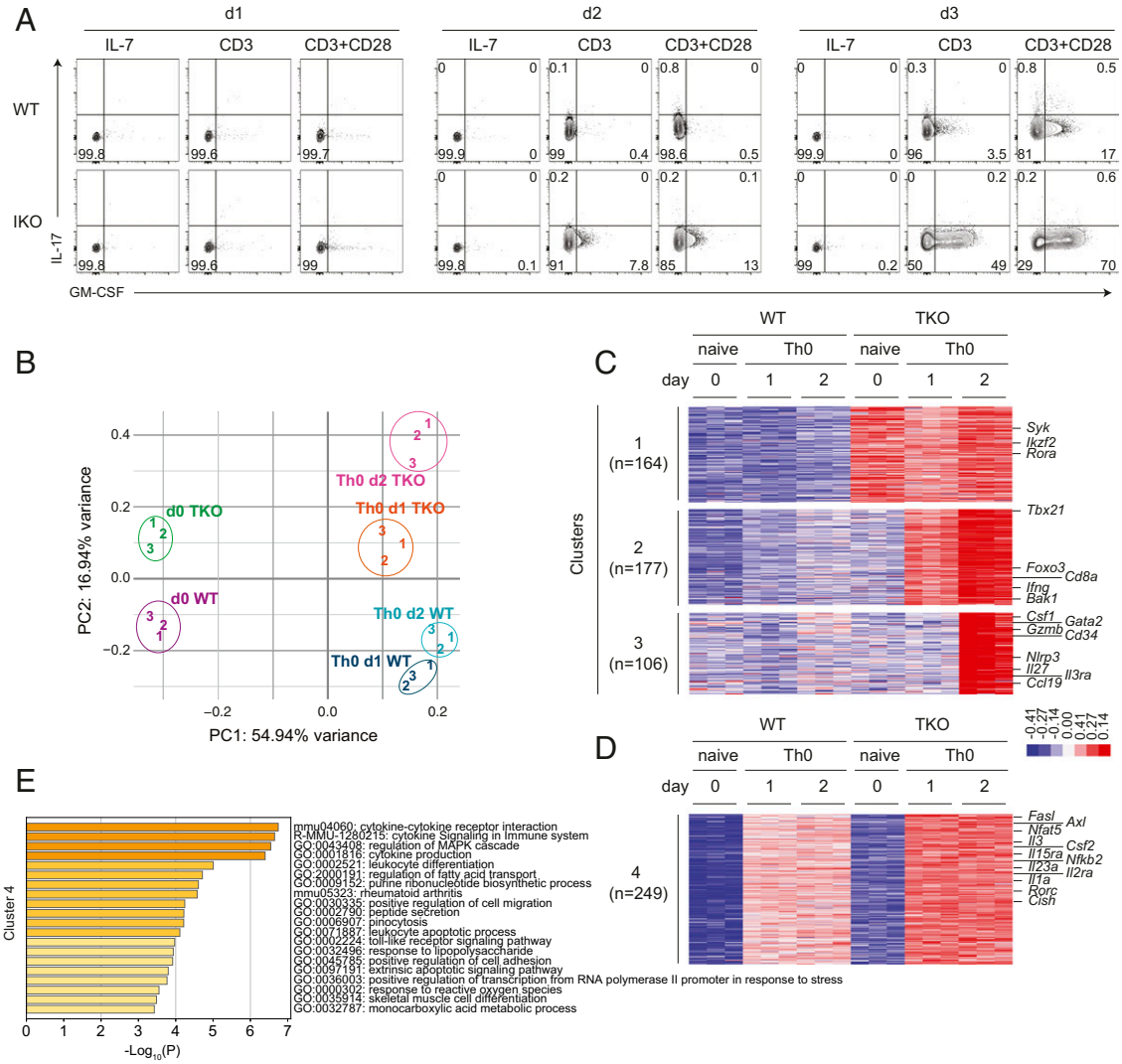

Fig. 3. Ikaros is required to limit GM-CSF expression upon T cell activation by TCR and CD28 signals. (*A*) Naive WT and IKO LN CD4$^+$ cells from tamoxifen-induced mice were cultured with IL-7 or activated with anti-CD3 ± anti-CD28 Abs for 1 to 3 d in the presence of QVD-OPh. A representative contour plot showing GM-CSF and IL-17 expression in live CD4$^+$ cells (n = 4) is shown. (*B*) PCA using expression data (RNA-seq) from WT and TKO T CD4$^+$ cells at day 0 and days 1 to 2 in Th0 cultures. The graph shows the first two principal components. (*C*) Heatmaps of three clusters of genes that were specifically increased in TKO cells compared to WT in Th0 cultures (K-means clustering). (*D*) Heatmap of a cluster of genes more increased in TKO cells compared to WT in Th0 cultures at day 1 and 2 (K-means clustering). (*E*) Metascape analysis of Gene Ontology term enrichment of genes from cluster 4 in *D*.

Ikaros Binding Correlates with Chromatin Closing. To determine if the changes in chromatin accessibility were due to Ikaros, we analyzed Ikaros binding on the chromatin of naive WT cells freshly isolated or activated in Th0 conditions for 1 d by chromatin immunoprecipitation sequencing (ChIP-seq). These analyses showed that the number and distribution of Ikaros peaks was similar in both conditions (*SI Appendix*, Fig. S13*A*). Interestingly, the intensity of Ikaros binding was globally reduced upon activation (Fig. 5*A*). At regions where Ikaros bound to WT chromatin, we observed a significant increase in chromatin accessibility in TKO cells (Fig. 5 *A* and *B*) along with increases in gene expression (Fig. 5*C*). These results suggested that Ikaros binding correlates with chromatin compaction and gene repression. Nonetheless, our analysis of the Ikaros-bound regions at loci containing *Csf2*, *Ifng*, *Il7r*, *Fasl*, and *Cish* [a positive control for Ikaros binding (39)] as well as those containing key regulatory proteins (i.e., *Foxo3*, *Tbx21*, *Nfat5*, *Rorc*) did not reveal obvious differences in the levels of ATAC-seq peaks between WT and TKO chromatin (Fig. 5*D* and *SI Appendix*, Fig. S13*B*). Thus, we concluded that Ikaros does not directly limit chromatin accessibility to repress a proinflammatory phenotype in activated T cells.

We found that Ikaros binds to the CNSa downstream of *Csf2*, which is an important enhancer for *Csf2* transcription (20) (Fig. 5*D*). To map the Ikaros binding site in this region, we performed an electrophoretic mobility shift assay with different probes containing the core Ikaros target motif GGAA. Of note, site 2 does not have an Ikaros core motif but corresponds to the summit of the Ikaros peak detected at day 0. As positive controls, Ikaros strongly bound the synthetic BS4 and the *Cish* sequences. Interestingly, Ikaros bound efficiently to the probe containing a tandem of sites (sites 5 and 6) present in the CNSa (Fig. 5*E*). Ikaros did not bind to site 4 alone. However, adding this sequence to the tandem sites promoted the appearance of a higher order complex, suggesting that additional proteins may be assembled with Ikaros. Mutagenesis analysis confirmed that sites 5 and 6 are crucial for Ikaros binding, while site 4 seems to be optional (Fig. 5*F*). Thus, Ikaros binding to the CNSa occurs in a region containing a repetition of Ikaros core sequences.

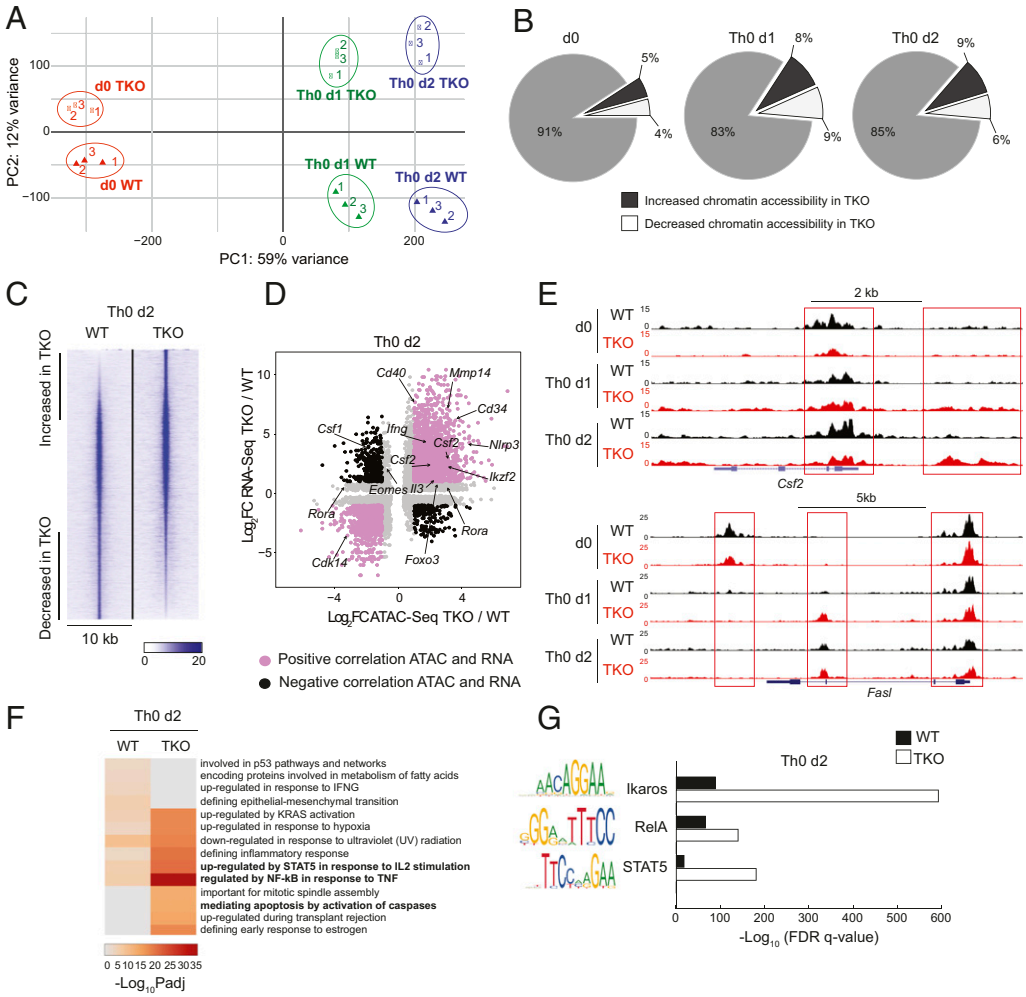

Fig. 4. Ikaros loss changes the landscape of chromatin accessibility in CD4$^+$ T cells. (*A*) PCA using ATAC-seq data from WT and TKO CD4$^+$ cells at day 0 and days 1 to 2 in Th0 cultures. The graph shows the first two principal components. Samples were obtained from three independent experiments. (*B*) Pie chart showing the distribution of ATAC-seq peaks in TKO cells compared to WT cells at day 0 and days 1 to 2 in Th0 cultures. Peaks increased in TKO cells (black; Log_2FC TKO/WT > 1 and padj ≤ 0.01) or decreased in TKO cells (white; Log_2FC TKO/WT < -1 and padj ≤ 0.01). The peaks that are not significantly changed between WT and TKO samples are shown in gray. (*C*) SeqMINER heatmap of all the 87,221 ATAC-seq peaks in WT and TKO cells at day 2 of Th0 cultures. (*D*) Integration of RNA-seq data with ATAC-seq data from TKO cells compared to WT cells at day 2 of Th0 cultures. Only the 8,572 peaks with a padj $\leq$ 0.05 from the ATAC-seq and RNA-seq analysis are shown. Among them, 3,576 peaks have a Log_2FC (TKO/WT) ≥ 1 or ≤ -1 and a Pearson correlation coefficient of 0.58 with a *P* value $< 2.2^{-16}$. Genes with a positive (purple) or a negative (black) correlation between ATAC-seq and RNA-seq data are highlighted. (*E*) Genome track view of ATAC-seq profiles of *Csf2* and *Fasl*. The University of California Santa Cruz Genome browser depicts the pooled profile of the three independent experiments in WT and TKO CD4$^+$ T cells at day 0 and days 1 to 2 in Th0 cultures. (*F*) Heatmap showing Gene Ontology terms enriched within genes associated with 4,486 ATAC-seq peaks significantly increased, and 2,774 peaks significantly decreased in TKO CD4$^+$ T cells in comparison to WT CD4$^+$ T cells at day 2 in Th0 cultures. Peaks significantly increased or decreased in the TKO were defined respectively with the following criteria: (Log_2FC(TKO/WT) $>$ 2 with a padj ≤ 0.01) and (Log_2FC(TKO/WT) < -2 with a padj ≤ 0.01). (*G*) Bar graph showing the significantly enriched transcription factor motifs identified from an Analysis of Motif Enrichment MEME motif search in ATAC-seq peaks found in WT and TKO CD4$^+$ T cells at day 2 in Th0 cultures. Significant peaks were selected as in *F*. Only some of the significantly enriched motifs are depicted.

Ikaros Antagonizes STAT5- and NFκB-Dependent GM-CSF Production in Activated T Cells. Because Ikaros, STAT5, and RelA motifs were enriched at regions of increased accessibility in Ikaros KO chromatin, we investigated the relationship between Ikaros and these pathways in regulating proinflammatory cytokine production. To assess the importance of STAT5, we evaluated the levels of STAT5 and activated STAT5 (p-STAT5) in naive CD4$^+$ T cells from tamoxifen-treated WT and IKO mice cultured for 2 d in Th0 condition, by Western blot. Interestingly, p-STAT5 levels were increased approximately threefold in IKO cells (Fig. 6*A*). To determine if increased STAT5 activity influences GM-CSF expression, we cultured these cells in Th0 conditions and a STAT5 inhibitor (STAT5i). Both *Csf2* mRNA and GM-CSF levels were reduced with increasing STAT5i concentrations (Fig. 6 *B* and *C*), suggesting that STAT5 activation plays a role in promoting GM-CSF production in Ikaros null cells.

To evaluate the importance of the NFκB pathway, we first treated WT and IKO cells with an inhibitor of IKK2 (IKK2i), a subunit of the IKK kinase that is required for the phosphorylation and degradation of the inhibitor of NFκB (IκBα), leading to NFκB activation. Strikingly, IKK2i treatment almost completely inhibited *Csf2* and GM-CSF expression in the activated IKO cells (Fig. 6 *D* and *E*). Similar results were obtained when we expressed a mutant IκBα protein that cannot be phosphorylated (IκBαSR) to block NFκB activation in WT and IKO cells (Fig. 6*F*). This showed that GM-CSF production was prevented greater than sevenfold in activated IKO cells expressing IκBαSR (and GFP), suggesting a pivotal role for NFκB activation in boosting GM-CSF expression in the absence of Ikaros.

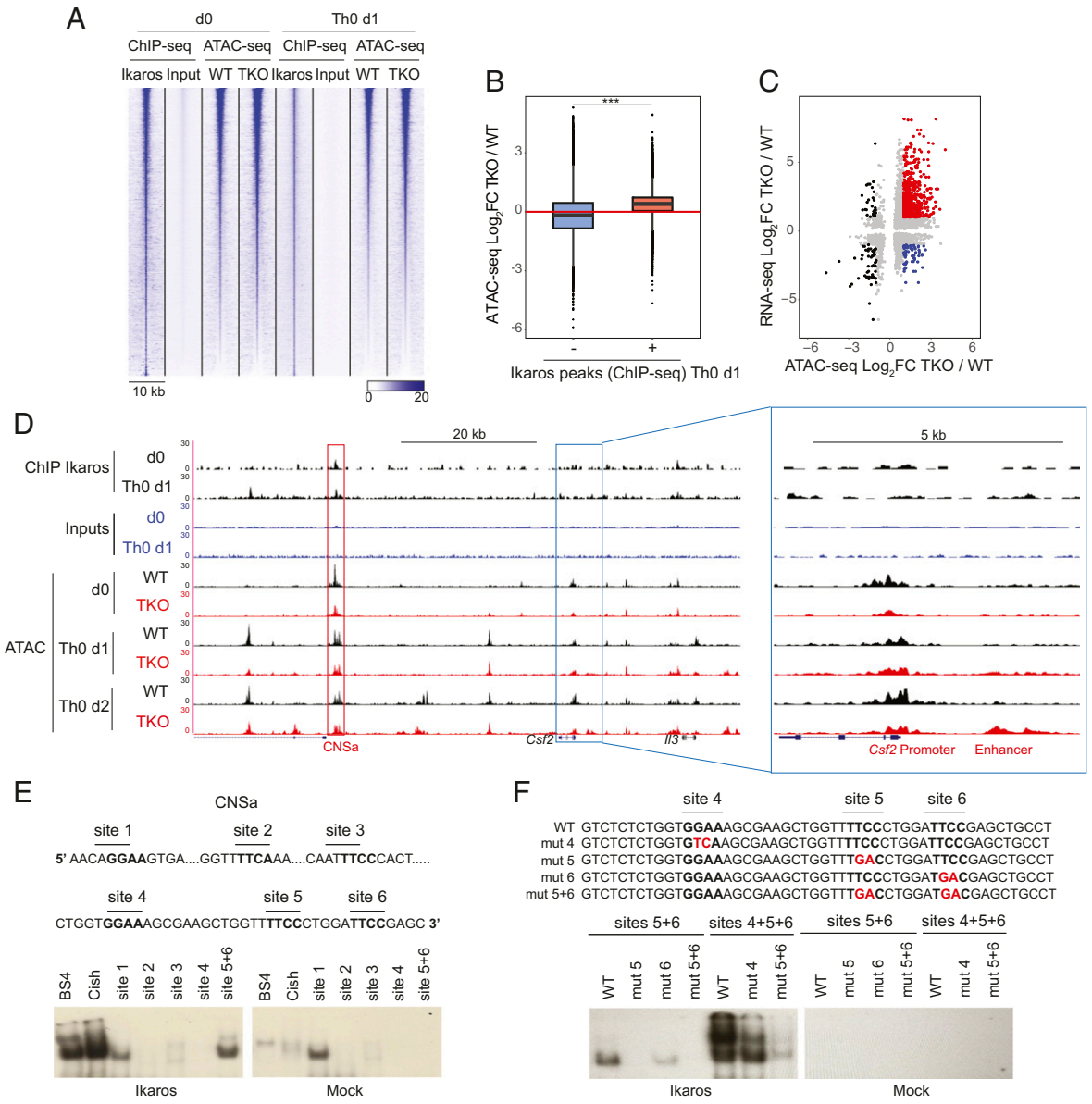

Fig. 5. Genome-wide ChIP-seq analysis of Ikaros binding in CD4$^+$ T cells. (*A*) SeqMINER heatmap showing the Ikaros peaks and the ATAC-seq peaks at day 0 and day 1 of Th0 cultures. (*B*) Boxplot showing the Log_2FC (TKO/WT) of all ATAC-seq peaks (78,378) in TKO versus WT cells that were bound (26,054) or not (52,324) by Ikaros in the Th0 day 1 condition (Mann–Whitney *U* test, $P < 2.2^{-16}$). (*C*) Integration of ATAC-seq data (Log_2FC TKO/WT) and RNA-seq data (Log_2FC TKO/WT) among the regions directly bound by Ikaros (26,054 peaks) at day 1 of Th0 culture. Gray dots: ATAC-seq regions with a more significant difference in accessibility between TKO and WT (padj ≤ 0.05) associated with a difference in the RNA-seq expression (padj ≤ 0.05). Red dots: ATAC-seq Log_2FC (TKO/WT) ≥ 1 and RNA-seq Log_2FC (TKO/WT) ≥1. Blue dots: ATAC-seq Log_2FC (TKO/WT) ≥ 1 and RNA-seq Log_2FC (TKO/WT) ≤ −1. Black dots: ATAC-seq Log_2FC (TKO/WT) ≤ −1 and RNA-seq Log_2FC (TKO/WT) ≤ −1 or ≥ 1. (*D*) University of California Santa Cruz Genome track view of Ikaros ChIP-seq profiles, showing the *Csf2* promoter and regulatory sequences in WT CD4$^+$ T cells at day 0 and day 1 of Th0 cultures and ATAC-seq of WT and TKO CD4$^+$ T cells at day 0 and days 1 to 2 in Th0 cultures. CNSa is shown on the *Left* and a focus on the *Csf2* promoter and enhancer is shown on the *Right*. (*E*) Binding of Ikaros to sites identified in the CNSa of the *Csf2* gene. Sites 2 and 3 correspond respectively to the summits of the Ikaros peak at day 0 and Th0 day 1. BS4 and Cish probes are used as positive controls. Nuclear extracts from Cos cells transfected with the empty vector were used as a negative control (Mock). (*F*) Analysis of Ikaros binding on CNSa probes with mutations on sites 4 to 6.

Together, these results indicated that Ikaros represses STAT5- and NFκB-dependent GM-CSF expression upon TCR and CD28 coactivation.

Reduced Expression of Ikaros in Human T Cells Leads to Increased GM-CSF Production. Finally, we asked if the function of Ikaros in inhibiting GM-CSF expression is conserved in human T cells. We activated peripheral blood lymphocytes (PBLs) from healthy donors with anti-CD3 ± anti-CD28 Abs in the presence or absence of Lenalidomide, a drug causing Ikaros degradation (40, 41). As expected, Ikaros expression was significantly decreased in Lenalidomide-treated cells (Fig. 7*A*). Strikingly, GM-CSF production and *CSF2* mRNA expression increased two- to threefold in Lenalidomide-treated cells, respectively at day 3 and day 2 of the culture (Fig. 7 *A* and *B*). These results therefore show that human T cells, like murine cells, require Ikaros to limit GM-CSF expression.

Discussion

In this study, we reveal Ikaros as a central negative regulator of the production of proinflammatory cytokines, particularly GM-CSF, which is linked to T cell pathogenicity. Ikaros promotes

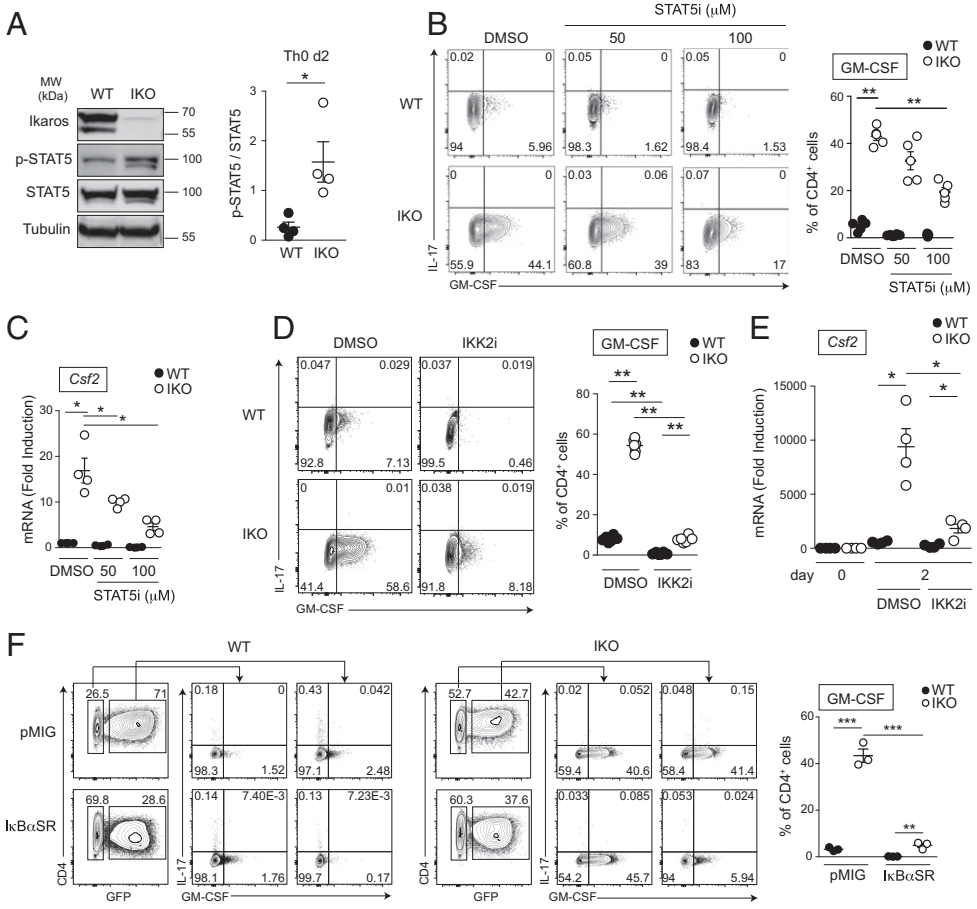

Fig. 6. GM-CSF production in Ikaros-deficient CD4$^+$ T cells depends on STAT5 and NFκB. (*A*, *Left*) Western blot of Ikaros and the phosphorylation of STAT5-Y694 in WT and IKO CD4$^+$ cells cultured 2 d in Th0 conditions with QVD-OPh. Tubulin and STAT5 are shown as loading controls. (*A*, *Right*) Ratio of STAT5-pY694/STAT5 in WT and IKO CD4$^+$ T cells at day 2 of Th0 cultures with QVD-Oph ($n = 4$; mean ± SEM). (*B*) Naive LN WT and IKO CD4$^+$ cells from tamoxifen-induced mice were cultured in Th0 conditions for 3 d with QVD-OPh in the presence of the STAT5 inhibitor (STAT5i) at indicated concentrations or dimethyl sulfoxide (DMSO) as a control. (*B*, *Left*) Representative contour plot showing GM-CSF and IL-17 expression in WT and IKO CD4$^+$ cells. (*B*, *Right*) Proportion of WT and IKO GM-CSF$^+$ CD4$^+$ T cells after 3 d of Th0 culture ($n = 4$ to 5; mean ± SEM). (*C*) RT-qPCR analysis of *Csf2* mRNA expression in WT and IKO LN naive CD4$^+$ cells cultured in Th0 conditions with QVD-OPh (day 2) in the presence of DMSO or STAT5i at indicated concentrations. *Csf2* mRNA expression is represented as fold induction with respect to the DMSO WT sample. Statistical significance for WT and IKO DMSO condition was analyzed by a Wilcoxon test. (*D*) Naive LN CD4$^+$ cells from tamoxifen-induced WT and IKO mice were cultured in Th0 conditions for 3 d with QVD-OPh in the presence of the IKK2 inhibitor (IKK2i; 2.5 μM) or DMSO as a control. (*D*, *Left*) Representative contour plot showing GM-CSF and IL-17 expression in WT and IKO CD4$^+$ cells. (*D*, *Right*) Proportion of WT and IKO GM-CSF$^+$ CD4$^+$ T cells after 3 d of Th0 culture with DMSO or IKK2i ($n = 6$; mean ± SEM). (*E*) RT-qPCR analysis of *Csf2* mRNA expression in naive LN WT and IKO CD4$^+$ cells harvested at day 0 or cultured in Th0 conditions with QVD-OPh (day 2) in the presence of DMSO or IKK2i (2.5 μM) and neutralizing anti-IFNγ and anti–IL-4 Abs (10 μg/mL). *Csf2* mRNA expression is represented as fold induction with respect to the DMSO WT sample ($n = 4$; mean ± SEM). (*F*) Naive LN CD4$^+$ T cells from tamoxifen-induced WT and IKO mice were activated with anti-CD3 + anti-CD28 Abs for 24 h and subjected to two rounds of infection with pMIG or IκBα super repressor (SR)/pMIG in the presence of QVD-OPh. At day 3, cells were stimulated with PMA, ionomycin, and GolgiPlug for 2 h, and IL-17 and GM-CSF expression was analyzed. (*F*, *Left*) Representative panels of GFP expression and of IL-17 and GM-CSF expression in GFP$^-$ and GFP$^+$ cells are shown. (*F*, *Right*) Proportion of WT and IKO GM-CSF$^+$ CD4$^+$ T cells infected with pMIG or IκBα super repressor after 3 d of Th0 culture ($n = 3$; mean ± SEM). Statistical significance was analyzed by parametric unpaired *t* test. Unless otherwise specified, statistical significance was analyzed by a Mann–Whitney *U* test (*$P \leq 0.05$, **$P \leq 0.01$, ***$P \leq 0.001$).

cTh17 development from naive CD4$^+$ T cells and is required during the polarization process. On the other hand, we find that Ikaros is required to suppress the development of proinflammatory T cells. In the absence of Ikaros, CD4$^+$ T cells polarized in Th17 cultures express proinflammatory cytokines resembling those expressed by pTh17, Th-GM, and Th17 cells infiltrating the central nervous system during EAE. Further, Ikaros-mediated repression of the pathogenic phenotype is independent of the polarization toward the Th17 fate, as TCR and CD28 coactivation can also induce this phenotype. Indeed, upon T cell activation, Ikaros represses transcription via chromatin remodeling and target gene binding, including at the *Csf2* locus. Importantly, we show that Ikaros also represses GM-CSF expression in TCR/CD28-activated human T cells. Thus, Ikaros is intimately tied to the balance between the conventional versus proinflammatory/pathogenic T cell phenotype in response to antigen.

Upon TCR and CD28 activation, loss of Ikaros leads to high *Ifng*, *Foxo3*, *Tbx21* (encoding T-bet), and *Eomes* expression in addition to *Csf2*. These genes have been described to drive Th1 pathogenicity in an EAE model (9), suggesting that Ikaros may repress more than one type of pathogenic T cell. We found that Ikaros binds to the promoters or enhancers of all of these loci. Ikaros has been described as a repressor of *Tbx21* and *Ifng* expression during Th2 polarization (42), but its potential role in limiting *Foxo3* and *Eomes* expression remains to be determined. We also observed that the activated Ikaros null T cells show an increased expression of *Maf* and *Prdm1*, which encode the Th2-associated factors Maf and Blimp-1, respectively. These transcriptional regulators have been shown to enhance *Csf2* expression

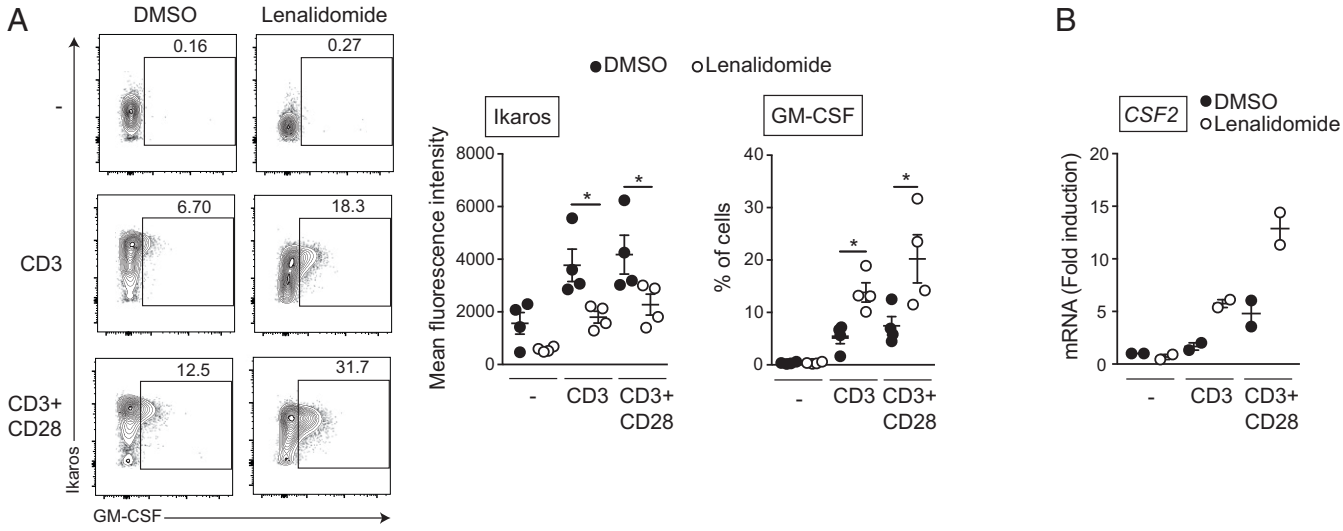

Fig. 7. Human cells require Ikaros to limit GM-CSF expression. Peripheral blood mononuclear cells were isolated from buffy coats of healthy donors and activated or not with anti-CD3 ± anti-CD28 Abs (10 μg/mL each) in the presence of Lenalidomide (10 μM) or DMSO as a control. (*A*, *Left*) Representative dot plot showing Ikaros and GM-CSF expression in DMSO and Lenalidomide-treated cells after 3 d of culture upon T cell activation or not. (*A*, *Middle*) Mean fluorescence intensity of Ikaros ($n = 4$; mean ± SEM). (*A*, *Right*) Proportion of GM-CSF$^+$ cells ($n = 4$; mean ± SEM). Statistical significance was analyzed by a paired Student *t* test (*$P \leq 0.05$). (*B*) RT-qPCR analysis of *CSF2* mRNA expression at day 2 of culture in DMSO and Lenalidomide-treated cells upon T cell activation or not ($n = 2$; mean ± SEM).

(43, 44). However, the expression of the genes encoding T-bet, Maf, and Blimp-1 was unchanged between WT and KO cells in Th17 conditions, suggesting that these factors do not contribute to GM-CSF expression in this context. How cell fate cues and lineage specific transcriptional regulators interfere with Ikaros-dependent repression of the proinflammatory phenotype remains to be determined. Cell fate specific conditions may indeed modulate the expression of pathogenic cytokines, as GM-CSF expression was no longer induced when the cells were stimulated in the presence of high concentrations of TGFβ1.

Our results suggest that Ikaros might inhibit GM-CSF production at three junctures. First, Ikaros may cooperate with NFκB to regulate *Csf2* (and likely *Il3*) transcription. We show that Ikaros binds the CNSa sequence 34 kb downstream of the *Csf2* gene, a site that was previously reported to be recognized by NFκB and Brg1 (a SWI/SNF remodeling ATPase) and important for *Il3* transcription (20). Since Ikaros is already present at this site in naive CD4$^+$ T cells and remains there following TCR + CD28 activation, it might disturb the recruitment of NFκB and Brg1, which binds only after activation (20). Second, Ikaros activity is negatively correlated with STAT5 phosphorylation, and active STAT5 is clearly required for strong GM-CSF expression in mutant cells, suggesting that Ikaros can affect the signaling cascades leading to STAT5 activation. As Ikaros binds close to the STAT5- (45) and NFκB-binding (20) sites on the CNSa, it could potentially dislodge them from their target sites or inhibit their function upon binding on adjacent sites. Third, Ikaros expression is associated with reduced chromatin accessibility at the *Csf2* enhancer where NFAT and AP1 can bind (19), even though Ikaros is not present at this region. However, by binding to distal regulatory regions, Ikaros could recruit the NuRD remodeling ATPase, Mi2β (46), or Polycomb Repressive Complex 2 (47) to the enhancer to promote chromatin compaction. Thus, Ikaros could block the access of critical transcription factors to the enhancer of *Csf2* by multiple ways.

How do the GM-CSF–producing T cells observed here fit into the current paradigms of pathogenic T cells? Our results suggest that Ikaros negatively regulates the pathogenic gene expression programs of pTh17, Th-GM, and pTh1 cells. In addition, under Th17 conditions, T cells lacking Ikaros strongly resemble Th17 cells infiltrating the central nervous system of mice during EAE (34). T cells expressing high levels of GM-CSF have been found in the cerebrospinal fluid of multiple sclerosis (MS) patients, and they have been shown to be pathogenic in murine EAE models (10, 11, 29, 48). Moreover, recent studies have highlighted GM-CSF as an essential Th cytokine that contributes to neuroinflammation in MS patients (12, 13). Importantly, we show that Ikaros also represses GM-CSF production in human T cells. It will therefore be of major interest to evaluate the functional consequences of Ikaros deficiency in models of autoimmunity. Interestingly, single-nucleotide polymorphisms in the *IKZF1* gene have been associated with autoimmune diseases such as systemic lupus erythematosus, inflammatory bowel disease, and primary Sjögren's syndrome (49–52), suggesting that genetic variations leading to changes in Ikaros levels may also contribute to the pathogenic programs in these patients. Lastly, pathogenic Th1 cells expressing high levels of GM-CSF$^+$ and IFNγ$^+$ have been found in the blood of patients with severe forms of Covid-19, requiring intensive care (14). These results could fit into our observation that Ikaros expression inversely correlates with the expression of a broad range of proinflammatory genes, including *Csf2* and *Ifng*. As such, Ikaros could be considered as an early prognosis biomarker, and screening T cells for its expression in Covid-19 patients could help predict the severity of the immune response.

Materials and Methods

Th0 and Th17 Cultures. Cell suspensions were prepared from total (mesenteric and peripheral) LNs, and cells were stained with anti-CD16/CD32 blocking Abs, anti-CD4, anti-CD8, anti-CD44, anti-CD25, anti-NK1.1, and anti-TCRγδ Abs in 1× phosphate-buffered saline (PBS) 10% heat-inactivated fetal calf serum (FCS) for 15 min on ice. Naive CD4$^+$ T cells (CD4$^+$CD8$^-$CD44$^{lo/-}$CD25$^-$NK1.1$^-$TCRγδ$^-$) were sorted on either a FACSAria II SORP or a FACSAria Fusion (BD Biosciences) cell sorter. Sort purity was >98%. Alternatively, CD4$^+$ T cells were enriched using the Dynabeads Untouched Mouse CD4 Cell Kit (Invitrogen) and stained with anti-CD44, anti-CD25, anti-NK1.1, and anti-TCRγδ Abs in 1× PBS 10% FCS for 15 min on ice, and naive CD4$^+$ T cells were sorted as previously described (35). Both protocols gave similar results for Th17 differentiation. For Th17 differentiation, naive CD4$^+$ T cells (4×10^4 cells/well) were activated with anti-CD3 and anti-CD28 (2 μg/mL each) Abs, both precoated overnight on a Nunc-Immuno 96-well plate (Thermo Scientific) in the absence or presence of IL-6

(10 ng/mL) and various TGFβ1 concentrations (0.0017 to 8 ng/mL) in 200 μl Iscove's Modified Dulbecco's Medium (IMDM) supplemented with 10% inactivated FCS, GlutaMAX-I, 100 U/mL Penicillin, 100 μg/mL Streptomycin, nonessential amino acids, sodium pyruvate, 10 mM Hepes, and β-mercaptoethanol (IMDM 10% FCS) as previously described (35). Similar results were obtained between human and mouse TGFβ1. When mentioned, naive $CD4^+$ T cells were activated with plate-bound anti-CD3 and anti-CD28 (2 μg/mL each), with or without IL-6 (10 ng/mL) and TGFβ1 (0.03 ng/mL) corresponding to Th17 and Th0 culture conditions, respectively. Where indicated, neutralizing anti-FasL Ab (20 μg/mL), neutralizing anti–IL-4 and anti-IFNγ Abs (10 μg/mL each), the pan-caspase inhibitor (QVD-OPh, 20 μM), and IL-7 (20 ng/mL) were added on naive $CD4^+$ T cells at day 0. At day 3, cells were stimulated with PMA plus ionomycin (0.5 μg/mL each) and GolgiPlug (1/1,000) for 2 h. When mentioned, cells were first stained with a Zombie Aqua fixable viability dye (BioLegend) according to the manufacturer's protocol and then stained with anti-CD4 and anti-CD8 Abs, fixed and permeabilized using the Foxp3 Fixation/Permeabilization Kit (eBiosciences), and stained with anti–IL-17, anti–GM-CSF, anti-IFNγ, and anti-Foxp3 Abs (where indicated). Protein expression was analyzed on live cells using the cytometer LSR II (BD Biosciences).

PBL Isolation, Activation, and Cytokine Measurement. Buffy coats were provided by the Etablissement Français du sang. Peripheral blood mononuclear cells were isolated using Ficoll-Paque PLUS (GE Healthcare) density gradient centrifugation. To eliminate most monocytes and platelets and obtain PBLs, one cycle of adherence to plastic for 1 h was performed. PBLs were cultured in Roswell Park Memorial Institute medium, 10% FCS, 1mM sodium pyruvate, 100 U/mL Penicillin, 100 μg/mL Streptomycin, and 10mM Hepes. For T cell activation, PBLs (5×10^4 cells/well) were activated with plate-bound anti-CD3 (OKT3) and anti-CD28 (10 μg/mL each) Abs on a Nunc-Immuno 96-well plate (Thermo Scientific) in the presence of Lenalidomide (10 μM; S1029, Selleckchem) or dimethyl sulfoxide as a control. After 3 d, cells were activated with PMA and ionomycin (0.5 μg/mL each) and GolgiPlug (1/1,000) for 4 h and then stained with a Zombie Aqua fixable viability dye (BioLegend) according to the manufacturer's protocol, fixed and permeabilized using the Foxp3 Fixation/Permeabilization Kit (eBiosciences), and stained with anti-human GM-CSF and anti-Ikaros Abs. Protein expression was analyzed on live cells using the cytometer LSR II (BD Biosciences).

Statistical Analysis. Statistical significance was analyzed by a Mann–Whitney *U* test to compare two experimental conditions unless indicated otherwise. Only statistical significances comparing the two conditions of interest are mentioned, unless indicated otherwise. Graphs and statistics were performed using Prism 7 (*$P \leq 0.05$, **$P \leq 0.01$, ***$P \leq 0.001$, and ****$P \leq 0.0001$).

Data Availability. Microarray data sets are accessible in the Gene Expression Omnibus data bank with the accession number GSE133878. The ChIP-seq, ATAC-seq, and RNA-seq data accession number is GSE157813. All other study data are included in the article and/or supporting information.

ACKNOWLEDGMENTS. We thank the Chan–Kastner laboratory for discussions; Claudine Ebel and Muriel Philipps for cell sorting help; Michael Gendron, Alexandre Vincent, William Magnant, and Sylvie Falcone for mouse husbandry; the GenomEast platform, a member of the France Génomique consortium (ANR-10-INSB-0009), for RNA-seq library preparation and sequencing; Doulaye Dembele for microarray data analysis and advice for statistical analyses; Christoph Borner for sharing plasmids; and Anne Dejean for helpful comments and critical reading of the manuscript. This study was funded by a grant from the Fondation ARC pour la Recherche sur le Cancer to C.C., an Agence Nationale de la Recherche (ANR) grant ANR-17-CE15-0023-02 to S.C., an Equipe Fondation pour la Recherche Médicale (FRM) grant EQU201903007812 to S.C., the grant ANR-10-LABX-0030-INRT, a French State fund managed by the ANR under the program Investissements d'Avenir ANR-10-IDEX-0002-02, and an equipment grant from the Ligue Régionale contre le Cancer du Grand Est to S.C. C.B. and G.M. were supported by pre-doctoral fellowships from the FRM (FDM20170637770) and the Ministère de l'Enseignement Supérieur, de la Recherche et de l'Innovation, respectively.

1. I. I. Ivanov *et al.*, The orphan nuclear receptor RORgammat directs the differentiation program of proinflammatory IL-17+ T helper cells. *Cell* **126**, 1121–1133 (2006).
2. X. O. Yang *et al.*, T helper 17 lineage differentiation is programmed by orphan nuclear receptors ROR α and ROR γ. *Immunity* **28**, 29–39 (2008).
3. M. J. McGeachy *et al.*, TGF-β and IL-6 drive the production of IL-17 and IL-10 by T cells and restrain T(H)-17 cell-mediated pathology. *Nat. Immunol.* **8**, 1390–1397 (2007).
4. X. Wu, J. Tian, S. Wang, Insight into non-pathogenic Th17 cells in autoimmune diseases. *Front. Immunol.* **9**, 1112 (2018).
5. K. Ghoreschi *et al.*, Generation of pathogenic T(H)17 cells in the absence of TGF-β signalling. *Nature* **467**, 967–971 (2010).
6. Y. Lee *et al.*, Induction and molecular signature of pathogenic TH17 cells. *Nat. Immunol.* **13**, 991–999 (2012).
7. L. Codarri *et al.*, RORγt drives production of the cytokine GM-CSF in helper T cells, which is essential for the effector phase of autoimmune neuroinflammation. *Nat. Immunol.* **12**, 560–567 (2011).
8. M. El-Behi *et al.*, The encephalitogenicity of T(H)17 cells is dependent on IL-1- and IL-23-induced production of the cytokine GM-CSF. *Nat. Immunol.* **12**, 568–575 (2011).
9. C. Stienne *et al.*, Foxo3 transcription factor drives pathogenic T Helper 1 differentiation by inducing the expression of Eomes. *Immunity* **45**, 774–787 (2016).
10. W. Sheng *et al.*, STAT5 programs a distinct subset of GM-CSF-producing T helper cells that is essential for autoimmune neuroinflammation. *Cell Res.* **24**, 1387–1402 (2014).
11. J. Rasouli *et al.*, A distinct GM-CSF^+ T helper cell subset requires T-bet to adopt a T_H1 phenotype and promote neuroinflammation. *Sci. Immunol.* **5**, eaba9953 (2020).
12. J. Komuczki *et al.*, Fate-mapping of GM-CSF expression identifies a discrete subset of inflammation-driving T helper cells regulated by cytokines IL-23 and IL-1β. *Immunity* **50**, 1289–1304.e6 (2019).
13. E. Galli *et al.*, GM-CSF and CXCR4 define a T helper cell signature in multiple sclerosis. *Nat. Med.* **25**, 1290–1300 (2019).
14. Y. Zhou *et al.*, Pathogenic T-cells and inflammatory monocytes incite inflammatory storms in severe COVID-19 patients. *Natl. Sci. Rev.* **7**, 998–1002 (2020).
15. A. Bonaventura *et al.*, Targeting GM-CSF in COVID-19 pneumonia: Rationale and strategies. *Front. Immunol.* **11**, 1625 (2020).
16. F. M. Lang, K. M. C. Lee, J. R. Teijaro, B. Becher, J. A. Hamilton, GM-CSF-based treatments in COVID-19: Reconciling opposing therapeutic approaches. *Nat. Rev. Immunol.* **20**, 507–514 (2020).
17. J. D. Fraser, A. Weiss, Regulation of T-cell lymphokine gene transcription by the accessory molecule CD28. *Mol. Cell. Biol.* **12**, 4357–4363 (1992).
18. P. N. Cockerill, M. F. Shannon, A. G. Bert, G. R. Ryan, M. A. Vadas, The granulocyte-macrophage colony-stimulating factor/interleukin 3 locus is regulated by an inducible cyclosporin A-sensitive enhancer. *Proc. Natl. Acad. Sci. U.S.A.* **90**, 2466–2470 (1993).
19. C. S. Osborne, M. A. Vadas, P. N. Cockerill, Transcriptional regulation of mouse granulocyte-macrophage colony-stimulating factor/IL-3 locus. *J. Immunol.* **155**, 226–235 (1995).
20. A. L. Wurster, P. Precht, M. J. Pazin, NF-κB and BRG1 bind a distal regulatory element in the IL-3/GM-CSF locus. *Mol. Immunol.* **48**, 2178–2188 (2011).
21. R. Schreck, P. A. Baeuerle, NF-kappa B as inducible transcriptional activator of the granulocyte-macrophage colony-stimulating factor gene. *Mol. Cell. Biol.* **10**, 1281–1286 (1990).
22. F. Jenkins, P. N. Cockerill, D. Bohmann, M. F. Shannon, Multiple signals are required for function of the human granulocyte-macrophage colony-stimulating factor gene promoter in T cells. *J. Immunol.* **155**, 1240–1251 (1995).
23. S. R. Himes, L. S. Coles, R. Reeves, M. F. Shannon, High mobility group protein I(Y) is required for function and for c-Rel binding to CD28 response elements within the GM-CSF and IL-2 promoters. *Immunity* **5**, 479–489 (1996).
24. R. S. Thomas *et al.*, ETS1, NFkappaB and AP1 synergistically transactivate the human GM-CSF promoter. *Oncogene* **14**, 2845–2855 (1997).
25. A. F. Holloway, S. Rao, X. Chen, M. F. Shannon, Changes in chromatin accessibility across the GM-CSF promoter upon T cell activation are dependent on nuclear factor kappaB proteins. *J. Exp. Med.* **197**, 413–423 (2003).
26. K. H. Brettingham-Moore, S. Rao, T. Juelich, M. F. Shannon, A. F. Holloway, GM-CSF promoter chromatin remodelling and gene transcription display distinct signal and transcription factor requirements. *Nucleic Acids Res.* **33**, 225–234 (2005).
27. F. S. Poke *et al.*, Depletion of c-Rel from cytokine gene promoters is required for chromatin reassembly and termination of gene responses to T cell activation. *PLoS One* **7**, e41734 (2012).
28. J. Yu *et al.*, T cell-intrinsic function of the noncanonical NF-κB pathway in the regulation of GM-CSF expression and experimental autoimmune encephalomyelitis pathogenesis. *J. Immunol.* **193**, 422–430 (2014).
29. R. Noster *et al.*, IL-17 and GM-CSF expression are antagonistically regulated by human T Helper cells. *Sci. Transl. Med.* **6**, 241ra80 (2014).
30. L. Y. Wong, J. K. Hatfield, M. A. Brown, Ikaros sets the potential for Th17 lineage gene expression through effects on chromatin state in early T cell development. *J. Biol. Chem.* **288**, 35170–35179 (2013).
31. C. Lyon de Ana, K. Arakcheeva, P. Agnihotri, N. Derosia, S. Winandy, Lack of Ikaros deregulates inflammatory gene programs in T cells. *J. Immunol.* **202**, 1112–1123 (2019).
32. J. J. Heller *et al.*, Restriction of IL-22-producing T cell responses and differential regulation of regulatory T cell compartments by zinc finger transcription factor Ikaros. *J. Immunol.* **193**, 3934–3946 (2014).
33. A.-S. Geimer Le Lay *et al.*, The tumor suppressor Ikaros shapes the repertoire of notch target genes in T cells. *Sci. Signal.* **7**, ra28 (2014).
34. R. Qiu *et al.*, Inhibition of glycolysis in pathogenic T_H17 cells through targeting a miR-21-Peli1-c-Rel pathway prevents autoimmunity. *J. Immunol.* **204**, 3160–3170 (2020).
35. A. Lainé *et al.*, Foxo1 is a T cell-intrinsic inhibitor of the RORγt-Th17 program. *J. Immunol.* **195**, 1791–1803 (2015).
36. L. Zhou *et al.*, TGF-β-induced Foxp3 inhibits T(H)17 cell differentiation by antagonizing RORgammat function. *Nature* **453**, 236–240 (2008).
37. L. E. Harrington *et al.*, Interleukin 17-producing CD4+ effector T cells develop via a lineage distinct from the T helper type 1 and 2 lineages. *Nat. Immunol.* **6**, 1123–1132 (2005).

38. S. P. Cullen *et al*., Fas/CD95-induced chemokines can serve as "find-me" signals for apoptotic cells. *Mol. Cell* **49**, 1034–1048 (2013).
39. C. D. S. Katerndahl *et al*., Antagonism of B cell enhancer networks by STAT5 drives leukemia and poor patient survival. *Nat. Immunol.* **18**, 694–704 (2017).
40. J. Krönke *et al*., Lenalidomide causes selective degradation of IKZF1 and IKZF3 in multiple myeloma cells. *Science* **343**, 301–305 (2014).
41. G. Lu *et al*., The myeloma drug lenalidomide promotes the cereblon-dependent destruction of Ikaros proteins. *Science* **343**, 305–309 (2014).
42. R. M. Thomas *et al*., Ikaros silences T-bet expression and interferon-gamma production during T helper 2 differentiation. *J. Biol. Chem.* **285**, 2545–2553 (2010).
43. J. Gilmour *et al*., Regulation of GM-CSF expression by the transcription factor c-Maf. *J. Allergy Clin. Immunol.* **120**, 56–63 (2007).
44. R. Jain *et al*., Interleukin-23-induced transcription factor blimp-1 promotes pathogenicity of T helper 17 cells. *Immunity* **44**, 131–142 (2016).
45. P. Li *et al*., STAT5-mediated chromatin interactions in superenhancers activate IL-2 highly inducible genes: Functional dissection of the Il2ra gene locus. *Proc. Natl. Acad. Sci. U.S.A.* **114**, 12111–12119 (2017).
46. J. Kim *et al*., Ikaros DNA-binding proteins direct formation of chromatin remodeling complexes in lymphocytes. *Immunity* **10**, 345–355 (1999).
47. A. Oravecz *et al*., Ikaros mediates gene silencing in T cells through Polycomb repressive complex 2. *Nat. Commun.* **6**, 8823 (2015).
48. J. Zhang *et al*., A novel subset of helper T cells promotes immune responses by secreting GM-CSF. *Cell Death Differ.* **20**, 1731–1741 (2013).
49. D. S. Cunninghame Graham *et al*., Association of NCF2, IKZF1, IRF8, IFIH1, and TYK2 with systemic lupus erythematosus. *PLoS Genet.* **7**, e1002341 (2011).
50. J.-W. Han *et al*., Genome-wide association study in a Chinese Han population identifies nine new susceptibility loci for systemic lupus erythematosus. *Nat. Genet.* **41**, 1234–1237 (2009).
51. V. Gateva *et al*., A large-scale replication study identifies TNIP1, PRDM1, JAZF1, UHRF1BP1 and IL10 as risk loci for systemic lupus erythematosus. *Nat. Genet.* **41**, 1228–1233 (2009).
52. S. Qu *et al*., Common variants near IKZF1 are associated with primary Sjögren's syndrome in Han Chinese. *PLoS One* **12**, e0177320 (2017).